NJC

Accepted Manuscript

This is an *Accepted Manuscript*, which has been through the Royal Society of Chemistry peer review process and has been accepted for publication.

Accepted Manuscripts are published online shortly after acceptance, before technical editing, formatting and proof reading. Using this free service, authors can make their results available to the community, in citable form, before we publish the edited article. We will replace this *Accepted Manuscript* with the edited and formatted *Advance Article* as soon as it is available.

You can find more information about *Accepted Manuscripts* in the Information for Authors.

Please note that technical editing may introduce minor changes to the text and/or graphics, which may alter content. The journal's standard Terms & Conditions and the Ethical guidelines still apply. In no event shall the Royal Society of Chemistry be held responsible for any errors or omissions in this *Accepted Manuscript* or any consequences arising from the use of any information it contains.

ROYAL SOCIETY OF CHEMISTRY

www.rsc.org/njc

Synthesis, Characterization of Nickel@Carbon Dots Hybrid Material and Application in Reduction Cr (VI)

Yali Guo, Dan Wang, Xiaoyu Liu, Xudong Wang, Weisheng Liu and Wenwu Qin*

[Sep 10, 2014]

Key Laboratory of Nonferrous Metal Chemistry and Resources Utilization of Gansu Province and State Key Laboratory of Applied Organic Chemistry, College of Chemistry and Chemical Engineering, Lanzhou University, Lanzhou 730000, P. R. China.

*To whom correspondence should be addressed. E-mail: W. Qin: qinww@lzu.edu.cn, Tel.: +86 -931-8912582; Fax: +86-931-8912582

Abstract

Nickel@carbon dots hybrid material (Ni@C-dots) was prepared through a simple reduction route and characterized by transmission electron microscopy (TEM), X-ray diffraction (XRD), Fourier-transform infrared spectroscopy (FTIR), X-ray photoelectron spectroscopy (XPS) and fluorescence spectroscopy. Additionally, the hybrid material was tested as a catalyst to reduce toxic Cr (VI) to nontoxic Cr (III), and UV-vis spectrophotometer was employed to monitor the reduction process. According to the results, Ni@C-dots hybrid material showed excellent hydrophilicity, good stability, and highly catalytic activity under room temperature.

1. Introduction

Carbon dots, a new type of photoluminescence (PL) carbon nanomaterial, were first obtained during purification of single-walled carbon nanotubes in 2004.[1] In the past decade, carbon dots had attracted numerous interests because of the high photostability and lack of cytotoxicity, and C-dots had been reported to possess many significant properties such as bioimaging, [2-6] sensing, [7-10] and photocatalysis *al etc*.[11-14] Moreover, C-dots was also as an excellent supports for nucleation and growth of the pristine nanocrystals due to the oxygen-containing functional groups on the surface.[15,16] On the other hand, metal nanoparticles (NPs) had emerged as a new class of materials and received considerable attention due to their unique electronic, optical, magnetic and catalytic properties.[17] However, few works had been reported about the metal nanoparticles supported on C-dots until now. [15,16,18,19] The combination of metal nanoparticles (Pd[15,16], Ag[16,18], Cu[16], Au[19]) and C-dots provide a successful integration

to the properties of the two components in the new hybrid materials.

To our knowledge, Cr (VI) was a leading contaminant in most hazardous waste sites and also known as a proven mutagen and a carcinogen. However, Cr (III) was believed to be an essential element to human metabolism.[20] Sadik et al. had used colloidal palladium nanoparticles to rapidly catalyze the reduction of Cr (VI) to Cr (III).[20] Goutam et al. had prepared Ni-RGO composite as a catalyst to reduce Cr (VI).[21] PdNP-supported mesoporous γ -Al_2O_3 film was also used as a catalyst for the reduction of Cr (VI).[22] In addition，nickel nanoparticles had been proved with important applications in catalysts and magnetic materials.[23] Herein, we had prepared a novel Ni@C-dots hybrid material by a simple reduction route in the presence of C-dots and the hybrid material was tested as a catalyst to reduce Cr (VI) to Cr (III).

Fluorescence spectroscopy was an attractive technique that had proven to be a powerful research tool in many research fields, such as chemistry, biology and materials science.[24-25] Because most catalysts and substrates had no fluorescence (detectable signal), fluorescence spectroscopy had rarely been applied to investigate of catalytic reactions. In principle, the intrinsic fluorescence of C-dots could be exploited to understand the photophysical properties of the catalyst and its catalytic mechanisms, which could be used to aid the design of new catalysts.

2. Experimental Section

2.1. Chemicals

Nickel (II) Chloride ($NiCl_2 \cdot 6H_2O$, Beijing Chemical Works, ⩾98%), sodium borohydride ($NaBH_4$, Sinopharm Chem. Reagent Co., Ltd, ⩾96%), citric acid

monohydrate (CA, ⩾ 99.5%), sodium hydroxide (NaOH, ⩾ 96%), hydrazine monohydrate ($H_2NNH_2 \cdot H_2O$, ⩾ 80%), formic acid (HCOOH, ⩾ 98.5%) and ethylene glycol ($HOCH_2CH_2OH$) were purchased from Tianjin Guangfu Reagent Company. Potassium dichromate ($K_2Cr_2O_7$, Tianjin chemical regent research institute, ⩾99%), nickel (II) acetylacetonate ($Ni(acac)_2$, Tokyo Chemical Industry Co., Ltd , 99%), oleylamine, (Beijing J & K Reagent Company), trioctylphosphine (TOP, Chengdu Aceda Chem. Reagent Co., Ltd, 90%). All reagents and solvents were of analytical grade and directly used without further purification.

2.2. Instrument

The transmission electron microscope (TEM) images were obtained from a JEM-2100 transmission electron microscope at an acceleration voltage of 120 kV. The samples were dispersed in ethanol and then dried on a holey carbon film Cu grid. Dynamic light scattered (DLS) was got on a BI-200SM (USA Brookhaven). XRD measurements were performed on a X-ray diffractometer (D/max-2400pc, Rigaku, Japan) with Cu Kα radiation (λ = 1.54178 Å), with operating voltage and current at 40 kV and 60 mA, respectively. The 2θ range was from 10 to 80 in steps of 0.02^o. For XRD observations, the samples were dispersed in aqueous solution and then dried on a glass slide. The Fourier transform infrared Spectroscopy (FTIR) spectra were measured by Nicolet 360 FTIR spectrometer with the KBr pellet technique. X-ray photoelectron spectra (XPS) were measured on a PHI-550 spectrometer by using the Mg Kα radiation (hν = 1253.6 eV) photoemission spectroscopy with a base vacuum operated at 300 W.

2.3. Steady-state UV − vis absorption and fluorescence spectroscopy

The absorbance of reduction process was recorded on a UV−visible spectrometer (Cary 100) at room temperature. The steady-state excitation and emission spectra were obtained from a FLS920 spectrofluorometer. Freshly prepared samples in 1 cm quartz cells were used to perform all UV–vis absorption and emission measurements.

2.4. Time-resolved fluorescence spectroscopy

Fluorescence lifetimes were measured on an Edinburgh Instruments FLS920 equipped with different light emitting diodes (excitation wavelength 330 nm and 360 nm), and used the time-correlated single photon counting technique[26] in 2048 channels at room temperature. The sample concentrations were adjusted to optical densities at the excitation wavelength (330 or 360 nm) < 0.1. The monitored wavelengths were 440nm, 450nm, and 460nm.

Histograms of the instrument response functions (using a LUDOX scatter) and sample decays were recorded until they typically reached 5.0 $\times 10^3$ counts in the peak channel. Obtained histograms were fitted as sums of the exponentials, using Gaussian-weighted nonlinear least squares fitting based on Marquardt–Levenberg minimization implemented in the sofware package of the instrument. The fitting parameters (decay times and preexponential factors) were determined by minimizing the reduced chi-square χ^2. An additional graphical method was used to judge the quality of the fit that included plots of surfaces (“carpets”) of the weighted residuals vs. channel number. All curve fittings presented here had χ^2 values < 1.1.

All measurements were done at 20^{o}C.

2.5. Preparation of C-dots

C-dots were prepared according to a reported method.[27] Citric acid monohydrate (2 g) was heated hydrothermally in a Teflon-equipped stainless-steel autoclave at 200 ^{o}C for 3h. After cooling to room temperature, the orange syrup product was neutralized with NaOH solution (1 mol L^{-1}) and further dialyzed against double distilled water through a dialysis membrane (MWCO of 1 KDa).

2.6. Synthesis of Ni@C-dots

Typically, an amount of nickel chloride was dissolved directly in ethylene glycol, and 10 ml $NiCl_2$•$6H_2O$ solution (45 mM) was mixed with 10 mL C-dots aqueous suspension in a 100 mL round bottom flask. Hydrazine hydrate (1.125 g) was then added to the mixture and maintained the concentration at 0.9 M. The mixture was kept vigorous stirring at 60 ^{o}C for 10 min. Subsequently, 5 mg mL^{-1} $NaBH_4$ was added dropwise to initiate the reaction. The royal purple solution was changed to dark which indicated the formation of Ni nanoparticles and kept stirring for another 1h at 60 ^{o}C. The crude product was isolated through centrifugation and washed with absolute alcohol. After that, the pure product was dissolved in aqueous solution (5 mg/mL) to generate the colloidal suspension of Ni@C-dots nanoparticles.

2.7. Reduction of Cr (VI)

A UV-vis spectrophotometer was used to monitor the reduction process by observing the mixture absorbance changes between 300 and 500 nm. Typically, 10mL Cr (VI) (1 mM), 1 mL formic acid (98.5%) and 9 mL H_2O were added to 50mL

beaker and adjusted the PH of the mixture to 2.0. The absorption spectrum was recorded just after preparation of this solution, 0.5 mL of colloidal Ni@C-dots nanoparticles were then added to the reaction mixture and absorption spectra were recorded in 2 min intervals. Similarly, the control experiments were also conducted.

3. Results and discussion

3.1. Characterization of C-dots and Ni@C-dots

The morphology and microstructure of the obtained C-dots and Ni@C-dots were characterized by TEM and dynamic light scattered (DLS). Fig. 1 demonstrated the morphology and the size of the prepared C-dots. The morphology of prepared C-dots was regularly spherical with an average diameter about 5 nm. Dynamic light scattering (DLS) analysis also showed that the average hydrodynamic diameter of C-dots was 4.4 nm (Figure. 1c).

The morphology of Ni@C-dots hybrid material was different comparing with that of C-dots. Fig. 2 showed the typical TEM images of the Ni@C-dots with core-shell nanostructures. It was formed with an ultrathin C-dot layer about 2 nm on the Ni nanoparticles (NPs) surface. Each composite NPs had a low contrast shell of continuous C-dot layers which wrapped a high contrast Ni core and indicated the formation of core-shell structures. Fig. 2c exhibited the HRTEM image of Ni@C-dots and it also demonstrated that the Ni cores were coated by ultrathin C-dots shells. The selected area electron diffraction (SAED) pattern of Ni@C-dots displayed the diffraction rings assigning to face-centered cubic (fcc) Ni (111) plane (Fig. S1†).

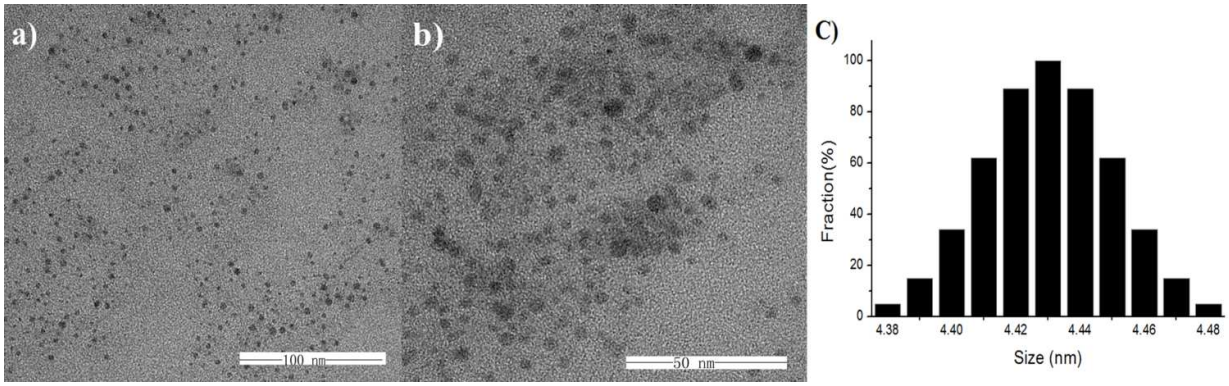

Fig. 1 (a, b) TEM images of C-dots with different magnifications. (c) Size distribution of C-dots.

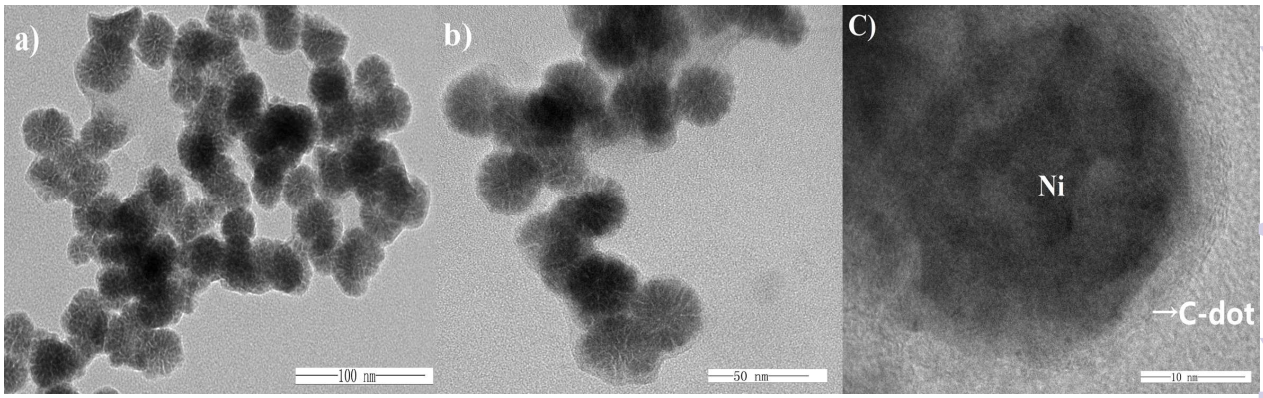

Fig. 2 (a, b) TEM images of Ni@C-dots with different magnification. (c) HRTEM image of Ni@C-dot nanoparticles.

The powder XRD spectra of C-dots showed a broad peak centred at 2θ= 23°(Fig. S2†), and Ni@C-dots showed a simple combination of an intense peak of C-dots at 2θ= 23° and small peaks of fcc nickel(2θ=44.5°)[28] (Fig. 3).

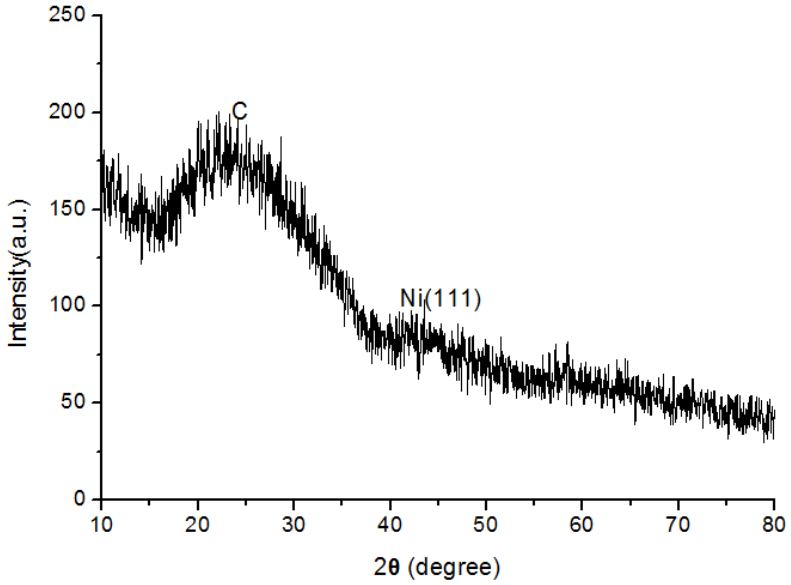

Fig. 3 XRD spectra of Ni@C-dots deposited on a glass slide.

Addtionally, the FTIR spectra showed that the C-dots exhibited characteristic stretching vibrations absorption bands of O-H at 3434 cm^{-1}, C=O at 1761 cm^{-1} and 1565 cm^{-1}. Notably, the C=O stretching peak of carbonyl at 1761 cm^{-1} was disappeared when they were involved in NiNP formation, which might attribute to the bonding interactions between the carboxylate groups and the metal (Fig. 4).[16]

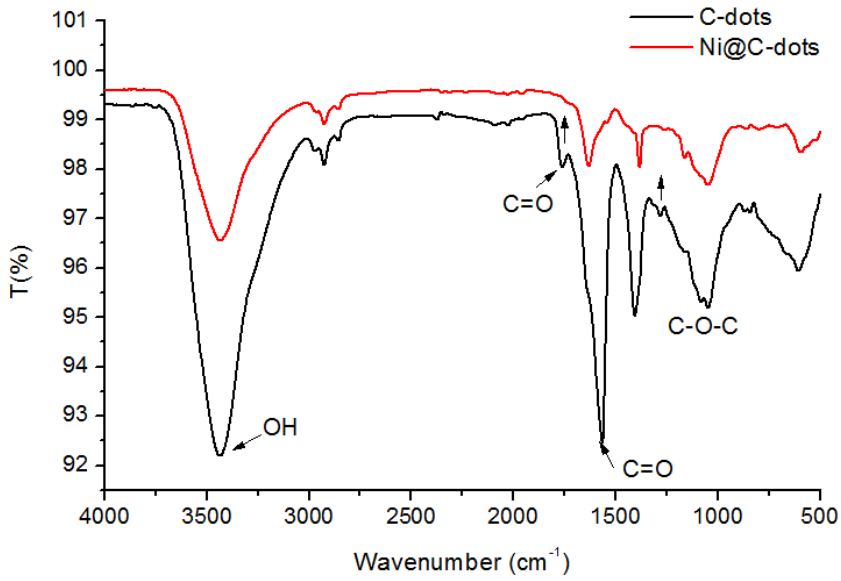

Fig. 4 FTIR spectra of C-dots and Ni@C-dots dried from aqueous suspension using KBr pellets.

In order to get further structural evidence, the XPS analysis of the Ni@C-dots was conducted (Fig. 5), and revealed three atom peaks at 289.5, 535.4 and 859.9 eV, which attributed to C, O and Ni atoms, respectively.[29]

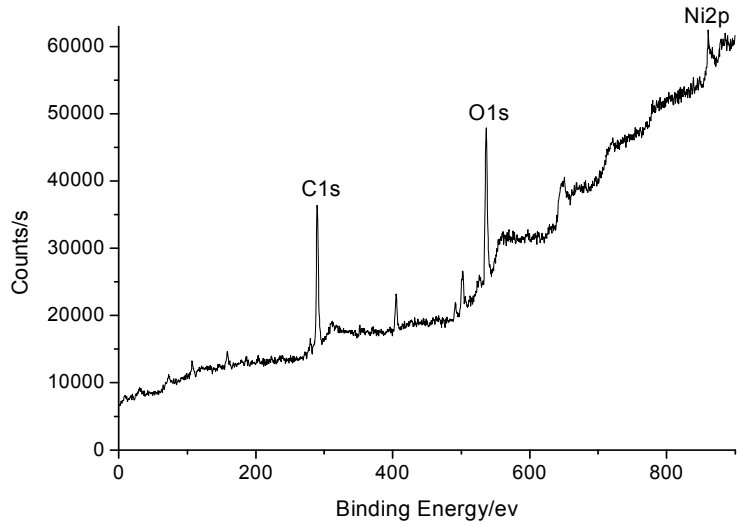

Fig. 5 XPS survey of the Ni@C-dots.

3.2 Optical properties

UV/Vis absorption spectra of C-dots dissolved in aqueous solution were depicted in Fig. 6a. The C-dots solution showed a broad UV/Vis absorption below 500 nm without any obvious peak, which was similar to the literature reported.[27] NiNPs had no ultraviolet absorption peak comparing with Au, Ag or other metal nanoparticles. For example, Au and Ag NPs had a typical plasmon absorption peak at 543 nm [19] and 418nm, [30] respectively. Hence, the UV/Vis absorption spectra of Ni@C-dots was

similar to the C-dots (Fig. 6a).

To further explore the optical properties of the prepared C-dots, a detailed photoluminescence study was carried out by using different excitation wavelengths (Fig. 6b), and the results showed that the corresponding emissions of the C-dots covered from blue to green wavelength range. The most intense PL of the C-dots dispersion appeared at 449 nm upon excitation at 340 nm. The emission bands shifted with the increased excitation wavelength, which revealed a distribution of the different surface energy traps toward the C-dots.[31,32] The fluorescence emission intensity of C-dots decreased following the increased excitation wavelength (longer than 340 nm). Recently, we had reported the photoluminescent properties of Ni@SiO_2–C-dots magnetic nanocomposite not only in solution but also in the solid state[29]. In this contribution, Ni@C-dots showed excellent hydrophilicity than Ni@SiO_2-C-dots magnetic nanocomposite. The photophysical properties of Ni@C-dots in water were quite different when compared with that of Ni@SiO_2-C-dots magnetic nanocomposite. The PL emission spectra and photoluminescent intensity of Ni@SiO_2-C-dots magnetic nanocomposite in ethanol could be observed with the change of the excitation wavelength. On the contrary, the formation of Ni@C-dots here was partly quenched the PL of C-dots as shown in Fig. 6c. It had been demonstrated that photoexcited C-dots could serve as both electron donors and electron acceptors and its photoluminescence could be quenched efficiently by either electron acceptor or donor molecules.[33] The photoinduced electron was transferred from C-dots shells to Ni cores or from Ni cores to C-dots

shells. Thus the formation of Ni@C-dots was partly quenched the photoluminescence of C-dots.

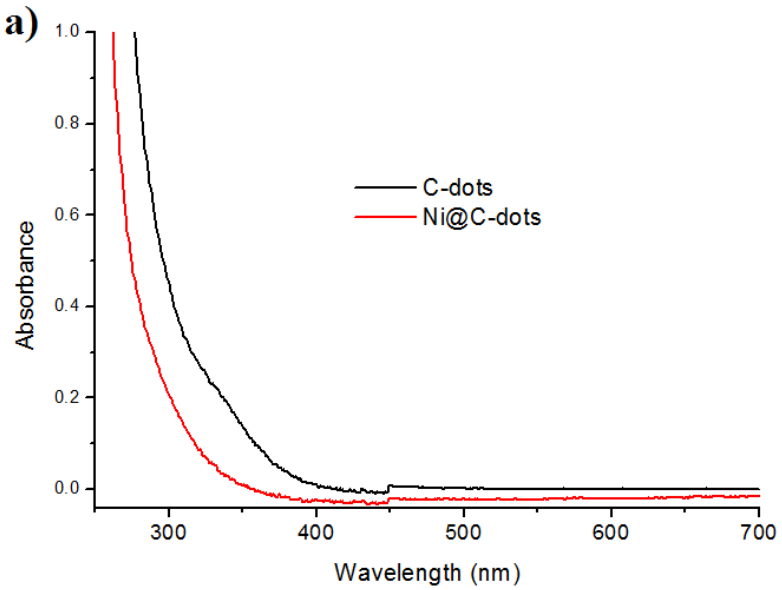

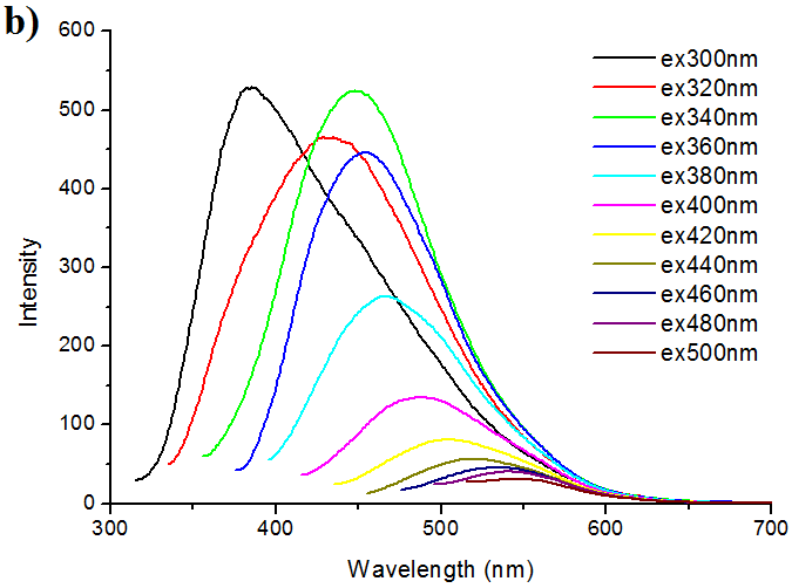

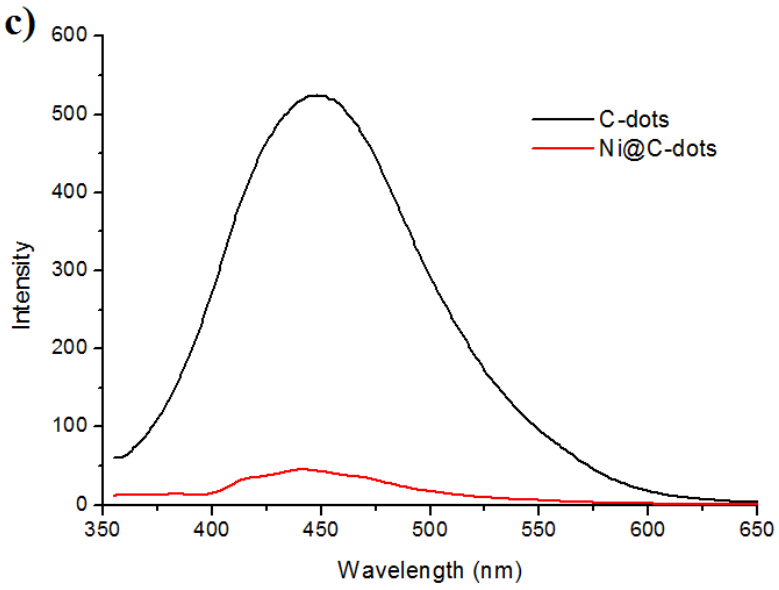

Fig. 6 (a) UV-visible absorption spectrum of C-dots and Ni@C-dots aqueous suspension . (b) PL spectra of C-dots aqueous suspension upon excitation at different excitation wavelengths. (c) PL spectrum of C-dots and Ni@C-dots aqueous suspension excited at 340 nm.

To investigate the fluorescence dynamics of C-dots and Ni@C-dots , fluorescence decay traces for the C-dots and Ni@C-dots in aqueous solution were collected as a function of emission wavelength λ_{em} through the single-photon timing technique. (Fig. 7, Table 1 and Fig. S3–S5†). Each fluorescence decay trace, was analyzed individually as a sum of two exponential function in terms of decay times τ_i and associated bi-exponential factors τ_i. Table 1 summarized the time resolved fluorescence data of C-dots and Ni@C-dots in aqueous solution.

Before an attempt was made to analyze the results, it was worth recapitulating the literature data on C-dots and Ni@SiO_2-C-dots magnetic nanocomposite. For C-dots in ethanol, a tri-exponential function (~1.0 ns, ~5.0 ns and ~13.0 ns) was used

to fit the decay at all three emission wavelengths. The fluorescence decay of Ni@SiO_2-C-dots nanocomposite powder in solid state at λ_{ex} = 330 or 360 nm can be described as bi-exponential function with the contributions of the τ_1 (~3.0 ns) and τ_2 (~9.0 ns) components, respectively. In ethanol, at the excitation of λ_{ex} = 330 or 360 nm, the fluorescence decays for Ni@SiO_2-C-dots magnetic clearly showed tri-exponential behaviour(~1.0 ns, ~5.0 ns and ~11.0 ns).[29] As we mentioned before, because of the C-dots and Ni@C-dots were not the same as the literature reported, the photophysical properties of Ni@C-dots in water were quite different when compared with that of Ni@SiO_2-C-dots magnetic nanocomposite. The fluoresence decay of C-dots in this article was fitted to the bi-exponential profile (λ_{ex}= 330 nm), the fast component (τ_1= ~1. 6ns) had the amplitude of about 39 %, whereas the contribution of the (τ_2= ~5.3ns) component was about 61 %. The different emission wavelengths of C-dots did not induce a obvious change in the fluorescence decay. The third lifetime could not be determined, which might due to it had an almost negligible contribution corresponding to the decay time. Fluoresence decay for Ni@C-dots also revealed bi-exponential profile, the longer lifetime decreased (~5.3 to ~2.5 ns) along with an decreased in the amplitude (~61% to ~13%). The shorter component almost remained constant (~1.6 to ~1.1 ns), the contribution for this component increased (~39% to ~87%). For the decay traces displayed in Figure. 7, it was cleared that the fluorescence lifetimes of Ni@C-dots decreased (become shorter) when compared with that of C-dots. Observation of this decreasing fluorescence lifetime for Ni@C-dots was in line with its lower fluorescence intensity than that of C-dots. The difference of

steady-state and time-resolved fluorescence spectrum properties between Ni@C-dots and C-dots indicated the formation of Ni@C-dots hybrid material.

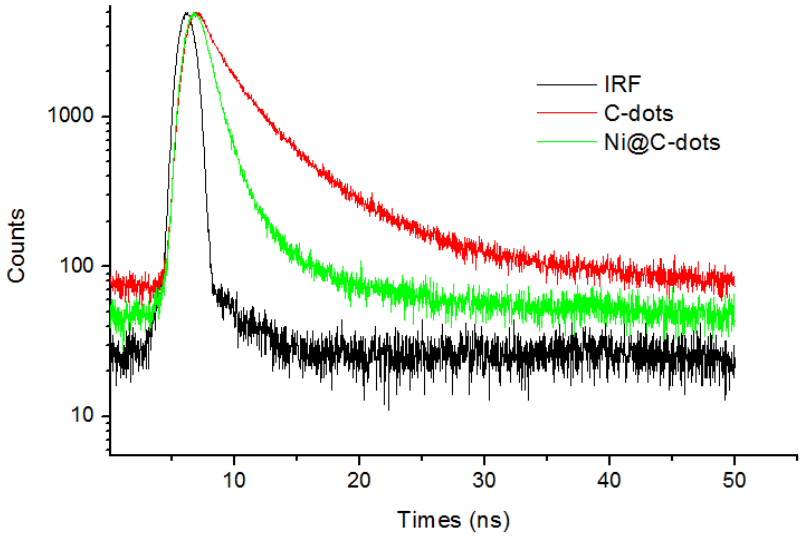

Fig. 7 Fluorescence decay profiles (λ_{ex}= 330 nm and λ_{em}= 450 nm) of C-dots and Ni@C-dots aqueous suspension.

Table 1 Photophysical Properties of C-dots and Ni@C-dots aqueous suspension. Decay times τ_1, τ_2 and the relative amplitude (%).

Compound	Excitation Wavelength /nm	Monitored Emission Wavelength /nm	τ_1/ns	τ_2/ns
C-dots	330	440	1.52(40.83 %)	5.21(59.17%)
		450	1.56(39.49%)	5.27(60.51%)
		460	1.61(38.00%)	5.39(62.00%)
	360	440	1.54(38.29%)	4.93(64.71%)
		450	1.51(37.50%)	4.95(62.50%)
		460	1.61(37.82%)	5.07(62.18%)
Ni@C-dots	330	440	1.03(87.80%)	3.95(12.20%)
		450	1.07(87.39%)	4.99(12.61%)
		460	1.07(87.36%)	5.11(12.64%)
	360	440	1.05(86.08%)	2.54(13.92%)
		450	1.07(86.80%)	2.57(13.20%)
		460	1.09(89.74%)	3.16(10.26%)

3.3 Catalytic properties

Ni@C-dots catalyzed formic acid to reduce Cr (VI) was monitored by using the UV−visible absorption spectrometer . The result displayed the changes in the intensity of the absorption peak of $Cr_2O_7^{2-}$at 350 nm. After 10min reaction, the adsorption peak of Cr (VI) was nearly disappeared and the color of the solution was changed from yellow to colorless in the presence of Ni@C-dots, confirming the complete reduction of Cr (VI) to Cr (III) (Fig. 8b).[21] The presence of Cr (III) in the colorless solution was confirmed by treating it with excess NaOH solution and the solution turned green due to the formation of hexahyroxochromate (III).[22] Otherwise, the blank experiment without the Ni@C-dots did not show any changes in color or adsorption peak of Cr (VI), which further proved the catalytic activity of Ni@C-dots (Fig. 8a). Control experiments for this reaction were also performed in the presence of bare Ni NPs [28] or pure C-dots under standard experimental conditions (S1.2.1-S1.2.2, Fig. S7-S8†). Fig.

9 showed the relationship between concentration ratio (C/C_0) of Cr (VI) and reaction time for different catalysts. The reduction rate was apparently slower in the presence of bare Ni NPs than that of the Ni@C-dots hybrid material. On the other hand, C-dots did not show any catalytic activity towards Cr (VI) reduction. The above results indicated that Ni@C-dots exhibit higher catalytic activity and faster reduction rate than NiNPs or C-dots. It was worthy to note that all of catalytic reduction experiments were performed at pH = 2.0, and the optimal pH had been previously proposed for more effective reduction of Cr (VI) to Cr (III).[34] $Cr_2O_7^{2-}$ converted to CrO_4^{2-} at higher PH and the UV-visible peak position of $Cr_2O_7^{2-}$ shifted toward higher wavelength with time due to the formation of CrO_4^{2-} ion. [21]

On the basis of the experiment results, a plausible mechanism for this redox reaction was proposed. Initially, HCOOH was adsorbed on the surface of Ni@C-dots and a redox reaction occured between Ni NPs and HCOOH on the C-dots surface. Then HCOOH decomposed to give CO_2 and hydrogen (H•). Subsequently, the free hydrogen atom reduced the species of Cr (VI) to Cr (III). Fig. S6† showed that the morphology of prepared bare Ni NPs was monodisperse and regularly spherical, and the morphology of Ni@C-dots hybrid material was different comparing with that of bare Ni NPs. The Ni@C-dots hybrid material was core-shell nanostructure and it was formed with an ultrathin C-dot layer around the Ni NPs surface (Fig. 2). Noteworthy, the reduction step was an electron-transfer process[21] and C-dots with excellent electron transfer property[35] could transfer the electron rapidly to reduce Cr (VI) at room temperature. For bare Ni NPs, there was no electronic transmission medium to

accelerate the electron transfer, hence, the rate of the reduction reaction dropt to a lower level comparing to the Ni@C-dots.

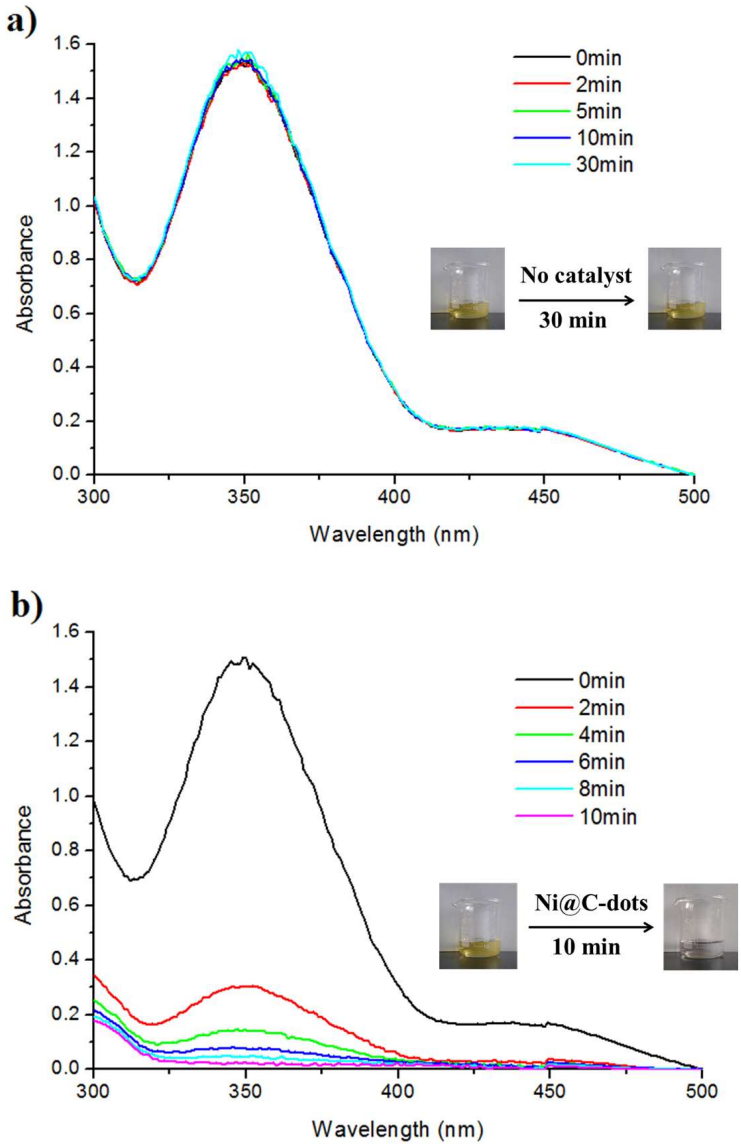

Fig. 8 UV−visible spectral evolution with time during the reduction of Cr (VI) by formic acid at room temperature in the absence (a) and in the presence (b) of Ni@C-dots. Inserts were visible color changes of Cr (VI) under daylight.

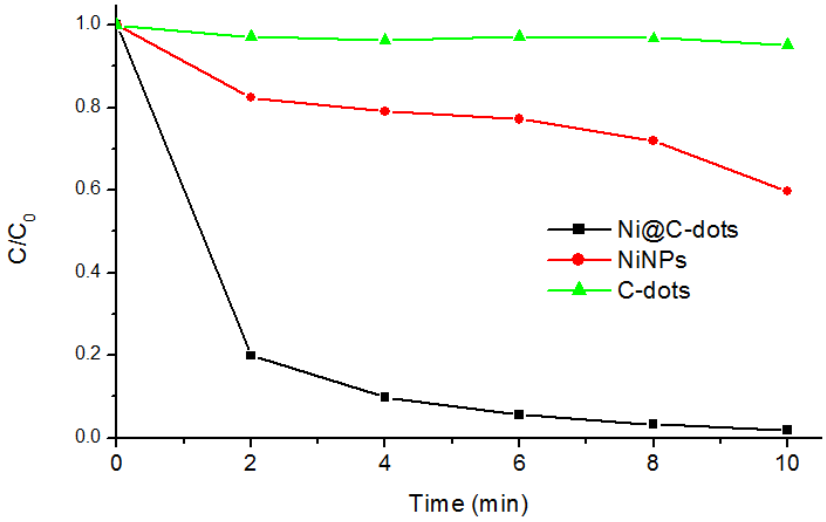

Fig. 9 The relationship between concentration ratio (C/C_0) of Cr (VI) and reaction time for different catalysts.

In order to study the stability of the catalyst, we studied the time resolved fluorescence and XPS to the catalyst after the catalytic reaction. Table 2 showed the time resolved fluorescence data of Ni@C-dots after catalytic reduction of Cr (VI).

Table 2 Photophysical Properties of Ni@C-dots after catalytic reduction of Cr (VI). Decay times τ_1, τ_2 and the relative amplitude (%).

Compound	Excitation Wavelength /nm	Monitored Emission Wavelength /nm	τ_1/ns	τ_2/ns
Ni@C-dots	330	440	0.87(91.52%)	3.47(8.48%)
		450	0.88(89.74%)	3.59(10.26%)
		460	0.87(89.34%)	3.74(10.66%)
	360	440	0.85(89.79%)	2.93(10.21%)
		450	0.86(88.30%)	3.10(11.70%)
		460	0.83(86.70%)	2.94(13.30%)

Compared with the data before catalytic reduction (Table 1), the time resolved fluorescence data of Ni@C-dots after reaction nearly kept constant when took into account the errors. It was indicated that Ni@C-dots hybrid material was steady and didn't take part in the reaction process. In order to get further information about the chemical state of Ni in the Ni@C-dots before and after catalytic reaction, we performed high resolution XPS analysis as shown in Fig. 10. HRXPS of Ni in Ni@C-dots before reduction revealed the peaks at 855.8 and 873.7 eV corresponding to 2p3/2 and 2p1/2, respectively. After reduction of Cr (VI), the peaks of Ni2P3/2 and Ni2P1/2 shifted to 856.9 and 875.1 ev, respectively. Compared to the data before reduction of Cr (VI), the HRXPS data of Ni nearly kept constant when took into account the errors, which suggested the stability and minimal structural changes of Ni nanoparticles during the catalytic reaction.

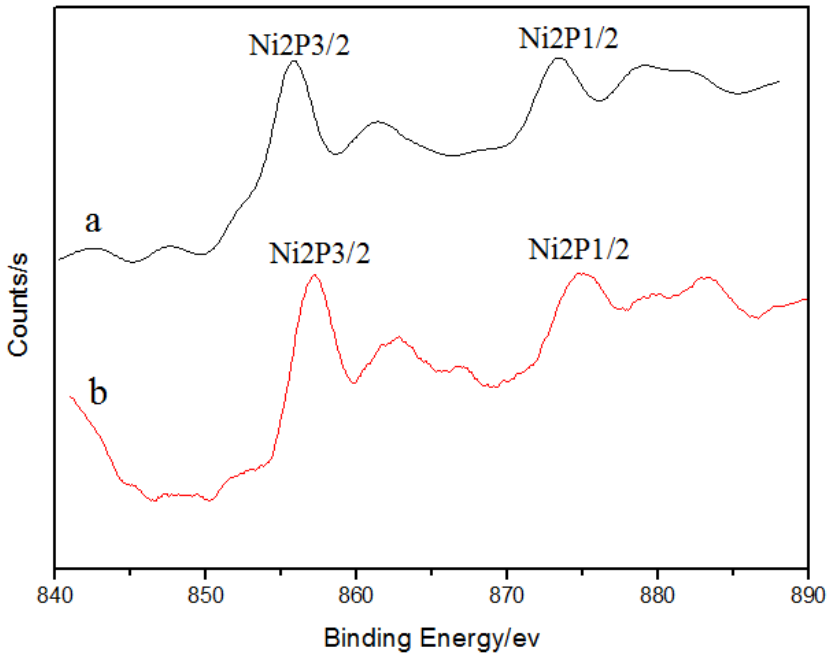

Fig. 10 HRXPS spectra of Ni in Ni@C-dots (a) before (b) and after reduction of

Cr (VI)

4. Conclusions

In summary, we had successfully prepared Ni@C-dots hybrid material with ultrathin carbon dots shells about 2 nm. The HRTEM clearly revealed the C-dots shells and Ni cores. C-dots served as an excellent supports for nucleation to grow nanoparticles and to prevent agglomeration. The morphology, structure and optical properties of the hybrid material were studied. Further catalytic experiments suggested that Ni@C-dots exhibited high catalytic activity towards reduction of Cr (VI) to Cr (III) by using formic acid as a reducing agent under room temperature. Our studies provide an approach to design novel functional composites and an effective catalyst to govern the water pollution.

Acknowledgements

This work was supported by the National Science Foundation for Fostering Talents in Basic Research of the National Natural Science Foundation of China (Grant no. J1103307) and the"International Cooperation Program of Gansu Province" (1104WCGA182). The authors would like to thank the Natural Science Foundation of China (no. 21271094), and this study was supported in part by the "Key Program of National Natural Science Foundation of China" (20931003).

Notes and References

1 X. Y. Xu, R. Ray, Y. L. Gu, H. J. Ploehn, L. Gearheart, K. Raker and W.A.Scrivens, *J. Am.Chem. Soc.*, 2004,**126**, 12736–12737.

2 L. Cao, X. Wang, M. J. Meziani, F. S.Lu, H. F.Wang, P. G. Luo, Y.Lin, B. A. Harruff, L. M. Veca, D. Murray, S. Y. Xie and Y. P. Sun, *J. Am. Chem. Soc.*, 2007,**129**, 11318-11319.

3 R. Liu, D. Wu, S. Liu, K. Koynov, W. Knoll and Q. Li, *Angew. Chem., Int. Ed.*, 2009, **48**, 4598–4601.

4 F. Wang, Z. Xie, H. Zhang, C. Y. Liu and Y. G. Zhang, *Adv. Funct. Mater.*, 2011, **21**, 1027-1031.

5 S. C. Ray, A. Saha, N. R. Jana and R. Sarkar, *J. Phys. Chem. C*, 2009 ,**113**, 18546–18551.

6 S. J. Zhu, J. H. Zhang, C. Y. Qiao, S. J. Tang, Y. F. Li, W. J. Yuan, B. Li, L. Tian, F. Liu, R. Hu, H. N. Gao, H. T. Wei, H. Zhang, H. C. Sun and B. Yang, *Chem. Commun.*, 2011, **47**, 6858–6860.

7 H. X. Zhao, L. Q. Liu, Z. D. Liu, Y. Wang, X. J. Zhao and C. Z. Huang, *Chem. Commun.*, 2011, **47**, 2604-2606.

8 W. L. Wei, C. Xu, J. S. Ren, B. L. Xu and X. G. Qu, *Chem. Commun.*, 2012, **48**, 1284-1286.

9 L. Zhou, Y. H. Lin, Z. Z. Huang, J. S. Ren and X. G. Qu, *Chem. Commun.*, 2012, **48**, 1147-1149.

10 S. Liu, J. Q. Tian, L. Wang, Y. W. Zhang, X. Y. Qin, Y. L. Luo, A. M. Asiri, A. O. Al-Youbi and X. P. Sun, *Adv. Mater.*, 2012, **24**, 2037-2041.

11 H. T. Li, X. D. He, Z. H. Kang, Y. Liu, J. L. Liu, S. Y. Lian, C. H. A. Tsang, X. B. Yang and S. –T. Lee, *Angew. Chem., Int. Ed.*, 2010, **49**, 4430-4434.

12 L. Cao, S. Sahu, P. Anilkumar, C. E. Bunker, J. Xu, K. A. S. Fernando, P. Wang, E. A. Guliants, K. N. Tackett and Y. P. Sun, *J. Am. Chem. Soc.*, 2011, **133**, 4754-4757.

13 B. Y. Yu and S. Y. Kwak, *J. Mater. Chem.*, 2012, **22**, 8345-9353.

14 Z. Ma, H. Ming, H. Huang, Y. Liu and Z. H. Kang, *New. J. Chem*., 2012, **36**, 861-864.

15 D. Dey, T. Bhattacharya, B. Majumdar, S. Mandani, B. Sharma and T. K. Sarma, *Dalton Trans.*, 2013, **42**, 13821-13825.

16 L. Tian, D. Ghosh, W. Chen, S. Pradhan, X. J. Chang and S. W. Chen, Chem. Mater., 2009, 21, 2803-2809.

17 P. D. Cozzoli, T. Pellegrino and L. Manna, *Chem. Soc. Rev.*, 2006, **35**, 1195-1208.

18 L. M. Shen, M. L. Chen, L. L. Hu, X. W. Chen and J. H. Wang, *Langmuir*, 2013, **29**, 16135-16140.

19 P. H. Luo, C. Li and G. Q. Shi, *Phys. Chem. Chem. Phys.*, 2012, **14**, 7360–7366.

20 M. A. Omole, I. O. K'Owino and O. A. Sadik, *Applied Catalysis B: Environmental*, 2007, **76**,

158–167.

21 K. Bhowmik, A. Mukherjee, M. K. Mishra and G. De, *Langmuir*, 2014, **30**, 3209-3216.

22 A. Dandapat, D. Jana and G. De, *Applied Catalysis A: General*, 2011, **396**, 34-39.

23 S. –H. Wu and D. –H. Chen, *J. Colloid. Interf. Sci.*, 2003, **259**, 282-286.

24 F. V. Bright, *Anal. Chem*., 1988, **60**, 1031A–1039A.

25 A. Tcherniak, C. Reznik, S. Link and C. F. Landes, *Anal. Chem*., 2009, **81**,746–754.

26 N. Boens, W. W. Qin, N. Basaric, J. Hofkens and M. Ameloot, *Anal. Chem.*, 2007, **79**, 2137-2149.

27 Y. Q. Dong, H. C. Pang, H. B. Yang, C. X .Guo, J. W. Shao, Y. W. Chi, C. M. Li and T. Yu, *Angew. Chem., Int. Ed.*, 2013, **52**, 7800-7804.

28 J. C. Park, H. J. Lee, J. U. Bang, K. H. Park and H. J. Song, *Chem. Commun.*, 2009, **25**， 7345-7347.

29 D. Wang, Y. L. Guo, W. S. Liu and W. W. Qin, *RSC Adv.*, 2014,**4**,7435-7439.

30 P. Raveendran, J. Fu and S. L. Wallen, *Green Chem*., 2006, **8**, 34-38.

31 X. F. Jia, J. Li and E. K. Wang, *Nanoscale*, 2012, **4**, 5572-5575.

32 Z. Lin, W. Xue, H. Chen and J. M. Lin, *Anal. Chem.*, 2011, **83**, 8245-8251.

33 X. Wang, L. Cao, F. S. Lu, M. J. Meziani, H. T. Li, G. Qi, B. Zhou, B. A. Harrufff, F. Kermarrec and Y. –P. Sun, *Chem. Commun*., 2009, **25**, 3774-3776.

34 F. Jiang, Z. Zheng, Z. Y. Xu, S. R. Zheng, Z. B. Guo and L. Q. Chen, *J. Hazard. Mater.*, 2006, **134**, 94-103.

35 H. T. Li, Z. H. Kang, Y. Liu, S. -T. Lee, *J. Mater. Chem*., 2012, **22**, 24230-24253.